

A flexible control strategy with overcurrent limitation in distributed generation systems



Doğan Çelik, Mehmet Emin Meral*

Department of Electrical and Electronics Engineering, Van Yuzuncu Yil University, Van, Turkey

ARTICLE INFO

Keywords:

Average filter
Distributed generation
Overcurrent controller
Flexible control

ABSTRACT

Distributed Generation (DG) systems are typically interfaced with distribution lines by modern power converter devices, which their controllers and dynamic behaviours are significantly influenced by unbalanced grid faults. The active and reactive power control with positive-negative sequences (PNS) is one of fundamental of power converter control under grid fault conditions. This paper proposes a reference current generator (RCG) based flexible power control strategy to enable regulation of active and reactive power with minimizing active and reactive power oscillations. Current limitation control is embedded into the RCG in order to keep maximum current injection in safety limitation for overcurrent protection under grid faults and harmonic distortions. The proposed control strategy has been also accomplished maximum active power and minimum reactive power transfer capability to electric grid. The analytical expression of active and reactive power oscillations depending on flexible control parameters are comprehensively investigated as theoretically and examined with simulations. Fractional order proportional integral (FOPI) controller is preferred to minimise steady state error of AC current regulation and provide faster processing time instead of conventional PI and proportional resonant (PR) controllers. An important contribution for similar previous studies is that PNS voltage and current components are separated by dual average filter based phase locked loop (DAPLL) which is firstly proposed in this paper. The performance of proposed controller is compared with multiple complex-coefficients filter (MCCF-PLL) based controller. Theoretical analysis and simulation results verify the correctness and effectiveness of the proposed solution.

1. Introduction

Distributed generation (DG) power systems technologies and alternative energy sources appear to be a viable option for addressing the increased demand for electricity which are directly connected to the consumers' load or dispatched to electric grid with power electronic devices at the low, medium and high voltage [1–4]. In order to maintain a stable power system in the interconnection DG power systems and transmission system operators, the impact of grid disturbances on the control of DG power systems need to be investigated [5,6]. The conventional control methods are mainly suitable for grid connected inverters (GCIs) under balanced conditions. However, electric grid voltage is affected by many factors such as overloads, grid faults and start-up of motors [7]. Therefore, the dynamic behaviour and control of the GCI can considerably influenced by unbalanced grid conditions. The GCI can exhibit undesirable performance such as overcurrent, power oscillations and DC bus voltage oscillations during grid faults [8].

Some recent studies have been analysed the flexible control

algorithms for the impact of grid faults on control of the GCI. While some researchers focused on excessive current stresses, the other researchers studied on maximum power delivery at rated inverter power capacity in [9–18]. Hence, the various reference current generators (RCGs) or reference power generators are presented to control the GCI for overcurrent prevention or maximum power delivery capability under grid fault conditions. In [9,11], the RCG based control algorithms have been developed for regulation of active and reactive powers. The analytic relationship between control parameters of positive–negative sequences (PNS) with power oscillations is well discussed and analysed. The overcurrent is achieved within safe current operation range. However, maximum injected current exceeds rated current in [10,11] because to avoid overcurrent phenomenon under grid faults, maximum injected current should be limited to rated current. The impact of harmonic distortions is not also considered. In [12], an advanced control algorithm is reported that peak current limitation is achieved by limited active power in wind turbine. Other interesting power control method is reported that a new vector transformation based

* Corresponding author.

E-mail addresses: dogancelik@yyu.edu.tr (D. Çelik), emeral@yyu.edu.tr (M.E. Meral).

<https://doi.org/10.1016/j.ijepes.2018.06.048>

Received 11 April 2018; Received in revised form 29 May 2018; Accepted 27 June 2018

Available online 24 July 2018

0142-0615/ © 2018 Elsevier Ltd. All rights reserved.

instantaneous p-q power control is enhanced in [13]. The system dynamics are considerably limited due to more computational burden and using more control modules in these methods. Moreover, conventional controllers such as proportional integral (PI) and proportional resonant (PR) controller are used for AC current regulation [9,14–17]. In particular, the impacts of harmonic distortions and voltage unbalanced factor are not taken into consideration in these control algorithms. The paper [18] offers sliding mode and Lyapunov function based control strategy. Active and reactive power oscillations are regulated and impacts of negative sequences are reported. However, current limitations are not surpassed and flexible control is not taken into consideration.

The sequences extractors are considerably essential control module to obtain the RCG. In addition, they are required to achieve accurate and fast dynamic behavior of GCI under grid faults and harmonic distortions. Some researchers have been reported various PLL based PNS extractors to generate reference current in the literature. Dual second-order generalized integrator (DSOGI) [15,19], time delay based PLL [20], third order sinusoidal integrator (TOSSI) [21] and multivariable based PLL (MVF) [14] are presented for detection of PNS components in stationary reference frame (STRF) and double synchronous reference frame (DSRF) [22], decoupled double synchronous reference frame (DDSRF) [23], differentiator method [24] are also presented for separation of PNS in synchronous reference frame (SRF) under unbalanced conditions. These methods are easily affected by voltage harmonic and some part of them has more the computational burden for signal processing. The speed of detection PNS components is slower. Moreover, using multiple filters increase the complexity of the control algorithm. The paper [25] only extracts positive sequences to generate reference current. The impacts of negative sequences on control signals and power oscillating components were not taken into account. In [26], multi complex coefficient filters (MCCF) based PNS extractor is presented to obtain fast and accurate PNS components. However, the impact of voltage harmonics, including many sub-modules and computational burden still seem problems. Among the above mentioned methods, DSC-PLL and MVF-PLL has the lowest dynamic response. On the other hand, the DSOGI provides much simpler structure for PNS extractor, but relatively slower response than proposed PLL. The MCCF-PLL has the transient response comparable with the TOSSI-PLL and DDSRF.

In this paper, the RCG based flexible control strategy has been carried out regulation of active and reactive powers with minimizing active and reactive power oscillations in GCI interfaced DG system under grid faults and harmonic distortions. The maximum current limitation control is inserted to the RCG for overcurrent protection. The impact of flexible control parameters on amplitudes of active and reactive power oscillations are examined and compared with MCCFF-PLL based RCG control strategy. Performance comparison of proposed control strategy is also comprehensively tested and reviewed with some previous studies. Fractional Order PI (FOPI) controller is used to achieve fast and accurate AC current regulation at steady state error instead of PI and PR controllers. Another key novelty is that PNS voltage-current components for the RCG are measured by proposed fast and robust dual average filter based PLL (DAPLL). The oscillations caused by grid faults and voltage harmonics on PNS orthogonal (d-q) signals are removed by proposed DAPLL. This paper provides some advantages in fourfold: (1) the PNS voltage-current components are separated by improved DAPLL, which provides fast response time, good robustness under grid faults and is not affected by low and high order harmonic components, (2) maximum active power and minimum reactive power are injected into utility grid without exceeding allowable phase current, (3) the proposed RCG based control algorithm is capable to deal with overcurrent limitation and (4) the analytical expression of active and reactive power oscillations based on flexible control parameters are comprehensively investigated as theoretically and verified with numerical and simulations results. Various cases are presented to support the validity and effectiveness of the proposed control strategy.

This paper is organized as six sections. Following the introduction section, the active and reactive power oscillation are formulated and analysed. In Section 3, the proposed flexible phenomenon based over-current limitation control and constant power control are introduced. In Section 4, proposed system is presented with PNS extractors and AC current regulation controller. Simulation results in Section 5 corroborate the claimed features of proposed solution. Performance comparison of proposed control strategy is discussed in Section 6. Section 7 concludes the paper and summarizes its main contribution.

2. The problem formulation with instantaneous power theory

Instantaneous active and reactive powers p, q are given in Eq. (1) [14];

$$p = v \cdot i = v_a i_a + v_b i_b + v_c i_c$$

$$q = v_{\perp} \cdot i = \frac{1}{\sqrt{3}}(v_b - v_c) i_a + (v_c - v_a) i_b + (v_a - v_b) i_c \quad (1)$$

where “ \perp ” denotes a vector derived from matrix transformation. v and v_{\perp} are orthogonal each other. Zero sequence components may be disregarded because θ of three wire structure. Three phase unbalanced grid voltage signals based on PNS components are written in matrix form.

$$v = \begin{bmatrix} v_a \\ v_b \\ v_c \end{bmatrix} = \begin{bmatrix} v^+ \sin(\theta^+) + v^- \sin(\theta^-) \\ v^+ \sin(\theta^+ - 2\pi/3) + v^- \sin(\theta^- - 2\pi/3) \\ v^+ \sin(\theta^+ + 2\pi/3) + v^- \sin(\theta^- + 2\pi/3) \end{bmatrix} \quad (2)$$

where positive phase angle θ^+ is equal to θ , which is measured from proposed PLL and negative phase angle θ^- equal to $-\theta$.

$$v_{\perp} = \frac{1}{\sqrt{3}} \begin{bmatrix} 0 & 1 & -1 \\ -1 & 0 & 1 \\ 1 & -1 & 0 \end{bmatrix} v \quad (3)$$

Considering three phase unbalanced grid voltage and currents, the active and reactive powers are written based on PNS components. Letters p, q are related to active and reactive power controls, which consist of active and reactive power oscillations, respectively.

$$p = v \cdot i = (v^+ + v^-)(i^+ + i^-)$$

$$q = v_{\perp} \cdot i = (v_{\perp}^+ + v_{\perp}^-)(i^+ + i^-) \quad (4)$$

Reformulated Eq. (4) in terms of i_d^{\pm} and i_q^{\pm} .

$$p = (v^+ + v^-)(i_d^+ + i_q^+ + i_d^- + i_q^-) = \underbrace{(v^+ i_d^+ + v^+ i_q^+ + v^- i_d^- + v^- i_q^-)}_P$$

$$+ \underbrace{(v^+ i_d^- + v^- i_d^+ + v^+ i_q^- + v^- i_q^+)}_{p_{2w}} \quad (5)$$

$$q = (v_{\perp}^+ + v_{\perp}^-)(i_d^+ + i_q^+ + i_d^- + i_q^-) = \underbrace{(v_{\perp}^+ i_d^+ + v_{\perp}^+ i_q^+ + v_{\perp}^- i_d^- + v_{\perp}^- i_q^-)}_Q$$

$$+ \underbrace{(v_{\perp}^+ i_d^- + v_{\perp}^- i_d^+ + v_{\perp}^+ i_q^- + v_{\perp}^- i_q^+)}_{q_{2w}} \quad (6)$$

where $v = v^+ + v^-$, $v_{\perp} = v_{\perp}^+ + v_{\perp}^-$, $v^+ = v_d^+ + v_q^+$ and $v^- = v_d^- + v_q^-$, similarly, for PNS current signals $i^+ = i_d^+ + i_q^+$ and $i^- = i_d^- + i_q^-$. p_{2w} and q_{2w} represent active and reactive power oscillations. From Eqs. (5) and (6) can be divided into two parts: one part is average power without oscillations, another part is active and reactive power oscillations. The detailed of power oscillations are given subsection in following.

2.1. Analysis of active-reactive power oscillations

Average active power P is obtained by Eqs. (4) and (5) under balanced conditions.

$$P = v^+ i^+ + v^- i^- \quad (7)$$

The active power oscillations are adjustable with flexible control

parameter μ_p . Active power oscillations based on PNS signals are derived from Eq. (5) under unbalanced grid conditions in following.

$$\begin{aligned} P_{2w} &= P_{2w,p} + P_{2w,q} \\ P_{2w,p} &= v^+ i_d^- + \mu_p v^- i_d^+ \\ P_{2w,q} &= v^+ i_q^- + \mu_p v^- i_q^+ \end{aligned} \quad (8)$$

The restriction parameter μ_p is a scalar coefficient that used as a weighting factor for elimination of active power oscillations. The relationship active power control parameter μ_p and PNS voltage components are written as follows;

$$\begin{aligned} v^+ i_d^- &= \mu_p v^- i_d^+ \quad -1 \leq \mu_p \leq 0 \\ v^+ i_q^- &= -\mu_p v^- i_q^+ \quad 0 \leq \mu_p \leq 1 \end{aligned} \quad (9)$$

Positive and negative orthogonal d-currents can be derived from Eq. (9) as

$$\begin{aligned} i_d^+ &= \frac{v^- i_d^-}{\mu_p \|v^-\|^2} v^+ \\ i_d^- &= \frac{\mu_p v^+ i_d^+}{\|v^+\|^2} v^- \end{aligned} \quad (10)$$

$\| \cdot \|$ is vector norm or magnitude of vector. By substituting Eq. (10) into active power P in Eq. (5), Eq. (11) is obtained in following.

$$\begin{aligned} i_d^+ &= \frac{P}{\|v^+\|^2 + \mu_p \|v^-\|^2} v^+ \\ i_d^- &= \frac{\mu_p P}{\|v^+\|^2 + \mu_p \|v^-\|^2} v^- \end{aligned} \quad (11)$$

Total active power current reference is given as follows:

$$i_{dref} = \frac{P}{\|v^+\|^2 + \mu_p \|v^-\|^2} (v^+ + \mu_p v^-) \quad (12)$$

where $i_{dref} = i_d^+ + i_d^-$. Average reactive power Q is derived from Eqs. (4) and (6) and given as follows;

$$Q = v_1^+ i^+ + v_1^- i^- \quad (13)$$

Reactive power oscillations based on PNS signals are derived from Eq. (6) under unbalanced conditions. Double frequency power oscillations $q_{2w,q}$ and $q_{2w,p}$ caused by unbalanced voltages are related with flexible control parameters μ_q as;

$$\begin{aligned} q_{2w} &= q_{2w,q} + q_{2w,p} \\ q_{2w,q} &= v_1^+ i_q^- + \mu_q v_1^- i_q^+ \\ q_{2w,p} &= v_1^+ i_d^- + \mu_q v_1^- i_d^+ \end{aligned} \quad (14)$$

Similar steps as described in active power oscillations, the relationship reactive power control parameter μ_q and PNS voltage components can be given as follows;

$$\begin{aligned} v_1^+ i_q^- &= \mu_q v_1^- i_q^+, \quad -1 \leq \mu_q \leq 0 \\ v_1^- i_d^- &= -\mu_q v_1^+ i_d^+, \quad 0 \leq \mu_q \leq 1 \end{aligned} \quad (15)$$

As abovementioned in active power control, similar steps are applied to reactive power control. Total reactive power reference current is given as follows:

$$i_{qref} = \frac{Q}{\|v^+\|^2 + \mu_q \|v^-\|^2} (v^+ + \mu_q v^-) \quad (16)$$

where $i_{qref} = i_q^+ + i_q^-$. In STRF, total active and reactive power reference current $i_{ref} = i_{dref} + i_{qref}$ is given as follows:

$$i_{ref} = \frac{P}{\|v^+\|^2 + \mu_p \|v^-\|^2} (v^+ + \mu_p v^-) + \frac{Q}{\|v^+\|^2 + \mu_q \|v^-\|^2} (v^+ + \mu_q v^-) \quad (17)$$

The total reference current in STRF form can be written in following.

$$\begin{aligned} \begin{bmatrix} i_{\alpha ref} \\ i_{\beta ref} \end{bmatrix} &= \frac{P}{\|v^+\|^2 + \mu_p \|v^-\|^2} \left(\begin{bmatrix} v_\alpha^+ \\ v_\beta^+ \end{bmatrix} + \mu_p \begin{bmatrix} v_\alpha^+ \\ v_\beta^+ \end{bmatrix} \right) \\ &+ \frac{Q}{\|v^+\|^2 + \mu_q \|v^-\|^2} \left(\begin{bmatrix} v_\alpha^+ \\ v_\beta^+ \end{bmatrix} + \mu_q \begin{bmatrix} v_\alpha^+ \\ v_\beta^+ \end{bmatrix} \right) \end{aligned} \quad (18)$$

2.2. Power quality characteristic

Generally, voltage balancing is proposed objectives. Actually, less amount of voltage unbalancing, is more desirable. Voltage unbalance factor [28] n_v is ratio of negative and positive sequence of voltage amplitudes as;

$$n_v = \frac{v^-}{v^+} = \sqrt{\frac{(v_d^-)^2 + (v_q^-)^2}{(v_d^+)^2 + (v_q^+)^2}} \quad (19)$$

Current unbalance factor as well as voltage unbalance factor based on PNS components can be written using IEEE true definition. One of main objectives is less unbalance factor [29]. Current unbalance factor is given as follows;

$$n_i = \frac{i^-}{i^+} = \sqrt{\frac{(i_d^-)^2 + (i_q^-)^2}{(i_d^+)^2 + (i_q^+)^2}} \quad (20)$$

where v_d^\pm , v_q^\pm , i_d^\pm and i_q^\pm are PNS voltage and current components. The average active power P is equal to the reference power P^{ast} and it is possible for average reactive power $Q^{ast} = Q$ at same time. The amplitudes of active and reactive power oscillations depend on flexible control parameters μ_p , μ_q , which vary interval of $[-1, 1]$. By substituting Eq. (18) into Eq. (5) and (6), the following equations can be obtained.

$$\begin{aligned} p &= P^* + \frac{P^*(1 + \mu_p) \|v^+\| \|v^-\|}{\|v^+\|^2 + \mu_p \|v^-\|^2} \cos(2wt + \theta_{PNS}) \\ &+ \frac{Q^*(1 - \mu_q) \|v^+\| \|v^-\|}{\|v^+\|^2 + \mu_q \|v^-\|^2} \sin(2wt + \theta_{PNS}) \end{aligned} \quad (21)$$

$$\begin{aligned} q &= P^* + \frac{Q^*(1 + \mu_q) \|v^+\| \|v^-\|}{\|v^+\|^2 + \mu_q \|v^-\|^2} \cos(2wt + \theta_{PNS}) \\ &+ \frac{P^*(1 - \mu_p) \|v^+\| \|v^-\|}{\|v^+\|^2 + \mu_p \|v^-\|^2} \sin(2wt + \theta_{PNS}) \end{aligned} \quad (22)$$

where $\theta_{PNS} = \tan^{-1} \left(\frac{P_{2w,p}}{P_{2w,q}} \right)$ and $\theta_{PNS} = \tan^{-1} \left(\frac{q_{2w,q}}{q_{2w,p}} \right)$ are phase angle between PNS components for active and reactive power oscillations, respectively. The phase angle between sequences is also given as $\theta_{PNS} = \theta^+ - \theta^-$. w is angle of fundamental frequency. Amplitudes of active and reactive power oscillations with Eqs. (23) and (24) are obtained from Eqs. (21) and (22);

$$|p_{2w}| = \sqrt{\left(\frac{P^*(1 + \mu_p) \|v^+\| \|v^-\|}{\|v^+\|^2 + \mu_p \|v^-\|^2} \right)^2 + \left(\frac{Q^*(1 - \mu_q) \|v^+\| \|v^-\|}{\|v^+\|^2 + \mu_q \|v^-\|^2} \right)^2} \quad (23)$$

$$|q_{2w}| = \sqrt{\left(\frac{Q^*(1 + \mu_q) \|v^+\| \|v^-\|}{\|v^+\|^2 + \mu_q \|v^-\|^2} \right)^2 + \left(\frac{P^*(1 - \mu_p) \|v^+\| \|v^-\|}{\|v^+\|^2 + \mu_p \|v^-\|^2} \right)^2} \quad (24)$$

For reactive power reference $Q^* = 0$, active and reactive power are controlled by only μ_p parameter. After substituting reactive power $Q^* = 0$ in Eqs. (23) and (24), simplified Eq. (25) are written in following.

$$\begin{aligned} |p_{2w}| &= \frac{P^*(1 + \mu_p) \|v^+\| \|v^-\|}{\|v^+\|^2 + \mu_p \|v^-\|^2} \quad -1 \leq \mu_p \leq 1 \\ |q_{2w}| &= \frac{P^*(1 - \mu_p) \|v^+\| \|v^-\|}{\|v^+\|^2 + \mu_p \|v^-\|^2} \end{aligned} \quad (25)$$

The ratio of active and reactive power oscillations [30] based on control parameters and voltage unbalance factor are rewritten as follows;

$$\begin{aligned} |p_{2\omega}| &= \frac{n_v(1+\mu_p)}{1+n_v^2\mu_p} - 1 \leq \mu_p \leq 1 \\ |q_{2\omega}| &= \frac{n_v(1-\mu_q)}{1+n_v^2\mu_q} - 1 \leq \mu_q \leq 1 \end{aligned} \quad (26)$$

3. Flexible control phenomenon

In this section, the main objective of the proposed controller contributes that a flexible control algorithm is capable of safely inject current at rated inverter capacity. The obtained active and reactive current references from PNS components are analysed with flexible control parameters. The RCG based control strategy and overcurrent limitation controller have been performed for maximum power delivery capability, minimizing active and reactive power oscillations and overcurrent protection.

3.1. The flexible constant active-reactive power control

The RCG is considerably crucial control module that determines the performances of the GCI during grid faults. The constant active and reactive powers are achieved by the RCG. In order to keep constant (maximum) power at level of inverter power capacity, the inverter current requires increasing. However, when active power production is high and exceeds rated (nominal) current, overcurrent issue occurs. Hence, active power curtailment should be occurred to avoid DC bus overvoltage and inverter tripping [11]. Three phase unbalanced grid voltages are converted to STRF with Clark transformations. The relationship between PNS components in SRF and STRF are given in following.

$$\begin{aligned} \begin{bmatrix} v_\alpha \\ v_\beta \end{bmatrix} &= \frac{2}{3} \begin{bmatrix} 1 & -\frac{1}{2} & -\frac{1}{2} \\ 0 & \frac{\sqrt{3}}{2} & -\frac{\sqrt{3}}{2} \end{bmatrix} \begin{bmatrix} v_a \\ v_b \\ v_c \end{bmatrix} \\ \begin{bmatrix} v_\alpha^+ \\ v_\beta^+ \\ v_\alpha^- \\ v_\beta^- \end{bmatrix} &= \begin{bmatrix} v^+ \sin(\theta^+) \\ -v^+ \cos(\theta^+) \\ v^- \sin(\theta^-) \\ v^- \cos(\theta^-) \end{bmatrix} \end{aligned} \quad (27)$$

The inverter output current is determined in following equations.

$$\begin{bmatrix} I_{\alpha ref} \\ I_{\beta ref} \end{bmatrix} = \begin{bmatrix} I_{\alpha(p)} + I_{\alpha(q)} \\ I_{\beta(p)} + I_{\beta(q)} \end{bmatrix} = \frac{2}{3} \frac{P^*}{v_\alpha^2 + v_\beta^2} \begin{bmatrix} v_\alpha \\ v_\beta \end{bmatrix} + \frac{2}{3} \frac{Q^*}{v_\alpha^2 + v_\beta^2} \begin{bmatrix} v_\beta \\ -v_\alpha \end{bmatrix} \quad (28)$$

where $I_{\alpha(p)}$, and $I_{\beta(p)}$ represent active power current and $I_{\alpha(q)}$ and $I_{\beta(q)}$ represent reactive power currents. P^* and Q^* are active and reactive power references and can be adjustable with inverter power capacity. The current references for active and reactive power can be calculated by PNS voltage components in STRF and obtained by substituting Eq. (28) into (27). Flexible control parameters are inserted in Eqs. (29) and (30). Inverter output current is obtained under unbalanced grid voltages in following.

$$\begin{cases} I_{\alpha(p)} = \frac{2}{3} \frac{P^*}{[(v_\alpha^+)^2 + (v_\beta^+)^2] + \mu_p [(v_\alpha^-)^2 + (v_\beta^-)^2]} [v_\alpha^+ + \mu_p v_\alpha^-] \\ I_{\beta(p)} = \frac{2}{3} \frac{P^*}{[(v_\alpha^+)^2 + (v_\beta^+)^2] + \mu_p [(v_\alpha^-)^2 + (v_\beta^-)^2]} [v_\beta^+ + \mu_p v_\beta^-] \end{cases} \quad -1 \leq \mu_p \leq 1 \quad (29)$$

$$\begin{cases} I_{\alpha(q)} = \frac{2}{3} \frac{Q^*}{[(v_\alpha^+)^2 + (v_\beta^+)^2] + \mu_q [(v_\alpha^-)^2 + (v_\beta^-)^2]} [v_\beta^+ + \mu_q v_\beta^-] \\ I_{\beta(q)} = \frac{2}{3} \frac{Q^*}{[(v_\alpha^+)^2 + (v_\beta^+)^2] + \mu_q [(v_\alpha^-)^2 + (v_\beta^-)^2]} [-v_\alpha^+ - \mu_q v_\alpha^-] \end{cases} \quad -1 \leq \mu_q \leq 1 \quad (30)$$

After PNS voltages in STRF are converted into SRF, the active and

reactive power current references based on PNS voltage components can be reformulated with flexible control parameters in Eqs. (31) and (32) [9].

$$\begin{cases} I_{\alpha(p)} = \frac{2}{3} \frac{P^*}{[\|v^+\|^2 + \mu_p \|v^-\|^2]} [v^+ \sin(\theta^+) + \mu_p v^- \sin(\theta^-)] \\ I_{\beta(p)} = \frac{2}{3} \frac{P^*}{[\|v^+\|^2 + \mu_p \|v^-\|^2]} [-v^+ \cos(\theta^+) + \mu_p v^- \cos(\theta^-)] \end{cases} \quad -1 \leq \mu_p \leq 1 \quad (31)$$

$$\begin{cases} I_{\alpha(q)} = \frac{2}{3} \frac{Q^*}{[\|v^+\|^2 + \mu_q \|v^-\|^2]} [-v^+ \cos(\theta^+) + \mu_q v^- \cos(\theta^-)] \\ I_{\beta(q)} = \frac{2}{3} \frac{Q^*}{[\|v^+\|^2 + \mu_q \|v^-\|^2]} [-v^+ \sin(\theta^+) - \mu_q v^- \sin(\theta^-)] \end{cases} \quad -1 \leq \mu_q \leq 1 \quad (32)$$

where $v^+ = \sqrt{(v_\alpha^+)^2 + (v_\beta^+)^2}$ and $v^- = \sqrt{(v_\alpha^-)^2 + (v_\beta^-)^2}$. The total references current can be given as follows;

$$\begin{bmatrix} I_{\alpha ref} \\ I_{\beta ref} \end{bmatrix} = \begin{bmatrix} I_{\alpha(p)} + I_{\alpha(q)} \\ I_{\beta(p)} + I_{\beta(q)} \end{bmatrix} = \begin{bmatrix} M_1 \sin(\theta^+ - \delta_1) + M_2 \sin(\theta^- - \delta_2) \\ -M_1 \cos(\theta^+ - \delta_1) + M_2 \cos(\theta^- - \delta_2) \end{bmatrix} \quad (33)$$

where the PNS active-reactive power current components is detailed by Eq. (34).

$$\begin{aligned} I_{\alpha(p)} &= I_{\alpha(p^+)} + I_{\alpha(p^-)} \\ I_{\alpha(q)} &= I_{\alpha(q^+)} + I_{\alpha(q^-)} \\ I_{\beta(p)} &= I_{\beta(p^+)} + I_{\beta(p^-)} \\ I_{\beta(q)} &= I_{\beta(q^+)} + I_{\beta(q^-)} \end{aligned} \quad (34)$$

where M_1 , M_2 , δ_1 and δ_2 is given in Eq. (35) as follows;

$$\begin{aligned} M_1 &= \sqrt{\left[\frac{v^+ P^*}{\|v^+\|^2 + \mu_p \|v^-\|^2} \right]^2 + \left[\frac{v^+ Q^*}{\|v^+\|^2 + \mu_q \|v^-\|^2} \right]^2} \\ \delta_1 &= \tan^{-1} \frac{Q^* [\|v^+\|^2 + \mu_p \|v^-\|^2]}{P^* [\|v^+\|^2 + \mu_q \|v^-\|^2]} \\ M_2 &= \sqrt{\left[\frac{\mu_p v^- P^*}{\|v^+\|^2 + \mu_p \|v^-\|^2} \right]^2 + \left[\frac{\mu_q v^- Q^*}{\|v^+\|^2 + \mu_q \|v^-\|^2} \right]^2} \\ \delta_2 &= \tan^{-1} \frac{\mu_q Q^* [\|v^+\|^2 + \mu_p \|v^-\|^2]}{\mu_p P^* [\|v^+\|^2 + \mu_q \|v^-\|^2]} \end{aligned} \quad (35)$$

3.2. Overcurrent limitation control

In the previous section, with increasing injected current under unbalanced grid faults, active and reactive powers are kept at reference power rating. And also, active-reactive power references are calculated by current references and grid voltage as mentioned below. However, to deal with excess current, active power curtailment should be occurred during grid faults. With inserting active and reactive power current references into Eqs. (29) and (30), the reference current components, Eqs. (36) and (37) are obtained [9]. The RCG components can be flexible adjusted by active and reactive power current references I_p^* , I_q^* and control parameters μ_p , μ_q .

$$\begin{cases} I_{\alpha(p)}^* = \frac{2}{3} \frac{I_p^* \sqrt{(v_\alpha^+)^2 + (v_\beta^+)^2}}{[(v_\alpha^+)^2 + (v_\beta^+)^2] + \mu_p [(v_\alpha^-)^2 + (v_\beta^-)^2]} [v_\alpha^+ + \mu_p v_\alpha^-] \\ I_{\beta(p)}^* = \frac{2}{3} \frac{I_p^* \sqrt{(v_\alpha^+)^2 + (v_\beta^+)^2}}{[(v_\alpha^+)^2 + (v_\beta^+)^2] + \mu_p [(v_\alpha^-)^2 + (v_\beta^-)^2]} [v_\beta^+ + \mu_p v_\beta^-] \end{cases} \quad -1 \leq \mu_p \leq 1 \quad (36)$$

$$\begin{cases} I_{\alpha(q)}^* = \frac{2}{3} \frac{I_q^* \sqrt{(v_\alpha^+)^2 + (v_\beta^+)^2}}{[(v_\alpha^+)^2 + (v_\beta^+)^2] + \mu_q [(v_\alpha^-)^2 + (v_\beta^-)^2]} [v_\beta^+ + \mu_q v_\beta^-] \\ I_{\beta(q)}^* = \frac{2}{3} \frac{I_q^* \sqrt{(v_\alpha^+)^2 + (v_\beta^+)^2}}{[(v_\alpha^+)^2 + (v_\beta^+)^2] + \mu_q [(v_\alpha^-)^2 + (v_\beta^-)^2]} [-v_\alpha^+ - \mu_q v_\alpha^-] \end{cases} \quad -1 \leq \mu_q \leq 1 \quad (37)$$

where $P^* = I_p^* v^+ = I_p^* \sqrt{(v_\alpha^+)^2 + (v_\beta^+)^2}$ and $Q^* = I_q^* v^+ = I_q^* \sqrt{(v_\alpha^+)^2 + (v_\beta^+)^2}$. Total reference currents are obtained by Eqs. (36) and (37) and given with Eqs. (38) and (39) in STRF as follows;

$$I_{\alpha ref} = \frac{2}{3} \frac{I_p^* \sqrt{(v_{\alpha}^+)^2 + (v_{\beta}^+)^2}}{[(v_{\alpha}^+)^2 + (v_{\beta}^+)^2] + \mu_p [(v_{\alpha}^-)^2 + (v_{\beta}^-)^2]} [v_{\alpha}^+ + \mu_p v_{\alpha}^-] + \frac{2}{3} \frac{I_q^* \sqrt{(v_{\alpha}^+)^2 + (v_{\beta}^+)^2}}{[(v_{\alpha}^+)^2 + (v_{\beta}^+)^2] + \mu_q [(v_{\alpha}^-)^2 + (v_{\beta}^-)^2]} [v_{\beta}^+ + \mu_q v_{\beta}^-] \quad -1 \leq \mu_p, \mu_q \leq 1 \quad (38)$$

$$I_{\beta ref} = \frac{2}{3} \frac{I_p^* \sqrt{(v_{\alpha}^+)^2 + (v_{\beta}^+)^2}}{[(v_{\alpha}^+)^2 + (v_{\beta}^+)^2] + \mu_p [(v_{\alpha}^-)^2 + (v_{\beta}^-)^2]} [v_{\beta}^+ + \mu_p v_{\beta}^-] + \frac{2}{3} \frac{I_q^* \sqrt{(v_{\alpha}^+)^2 + (v_{\beta}^+)^2}}{[(v_{\alpha}^+)^2 + (v_{\beta}^+)^2] + \mu_q [(v_{\alpha}^-)^2 + (v_{\beta}^-)^2]} [-v_{\alpha}^+ - \mu_q v_{\alpha}^-] \quad -1 \leq \mu_p, \mu_q \leq 1 \quad (39)$$

It should be reported that if injected active-reactive power keep at desired value, overcurrent issue will occur. In order to ensure overcurrent issue in safety limit, injected power should be decreased. The measured maximum injected current value from inverter output can be obtained by Eq. (40) as follows;

$$I_{max} = \frac{2}{3} \sqrt{\left[\frac{I_p^* \|v^+\|^2}{\|v^+\|^2 + \mu_p \|v^-\|^2} \right]^2 + \left[\frac{I_q^* \|v^+\|^2}{\|v^+\|^2 + \mu_q \|v^-\|^2} \right]^2} + \frac{2}{3} \sqrt{\left[\frac{\mu_p I_p^* \|v^+ \| \|v^-\|}{\|v^+\|^2 + \mu_p \|v^-\|^2} \right]^2 + \left[\frac{\mu_q I_q^* \|v^+ \| \|v^-\|}{\|v^+\|^2 + \mu_q \|v^-\|^2} \right]^2} \quad -1 \leq \mu_p, \mu_q \leq 1 \quad (40)$$

As seen from Fig. 1a with numerical values, when $\mu_p = -1$ and $n_v = 0.36$, $|p_{2w}| = 0$ and $|q_{2w}| = 0.82$. Similarly, when $\mu_p = +1$ and $n_v = 0.36$, $|p_{2w}| = 0.67$ and $|q_{2w}| = 0$. The active and reactive power oscillations are not influenced by μ_q due to reference reactive power Q^* is selected as 0. From $\mu_p = -1$ to $\mu_p = 1$, amplitude of active power oscillation is increased and similarly, amplitude of reactive power oscillation is decreased (see Fig. 2).

As shown in Fig. 1c and d and Eq. (40), the amplitudes of I_{max} changes as function of positive sequence v^+ , negative sequence v^- and flexible control parameters μ_p and μ_q . Simulation result shows that the

minimum current is 0.66 p. u value, with $\mu_p = 0$ and $\mu_q = 0$. Maximum injected current is 1 p. u value with $\mu_p = 1$. Therefore, the selection of μ_p and μ_q values involves with the trade-off between p_{2w} , q_{2w} and I_{max} . Variation of flexible control parameters μ_p , μ_q and negative sequence voltage affect the maximum injected current. When reactive power current reference I_q^* is selected as 0, maximum current is only depend on active power current reference I_p^* (Fig. 1c). However, as depicted in Fig. 1d, when reactive power current reference is greater than zero ($I_q^* = 0.2$), variation of maximum injected current, I_{max} depends on both references.

Flexible control parameters affect the power oscillations. μ_p and μ_q is an integer in the interval of [-1, 1]. As shown in Table 1, μ_p is used to select the required control targets. In proposed system, only one flexible control parameter μ_p is used. When $\mu_p = 0$, the injected current is balanced. Similarly, when $\mu_p = \pm 1$ are used to eliminate active and reactive power oscillations. Therefore, it is adjustable to customize the control objectives for different demands. The amplitude of the active and reactive power oscillations are summarized under variation of control parameter in Table 1.

4. The proposed system

The fast and robust PNS components are considerably essential to obtain RCG. In this paper, the measured PNS components from proposed DAPLL is embedded in RCG control module to deal with overcurrent phenomenon, provide maximum power delivery and minimizing active and reactive power oscillations in GCI interfaced DG system. The proposed controller ensures better solution than MCCF based overcurrent limitation controller in terms of oscillations caused by voltage harmonics and grid faults. In particular, proposed DAPLL based PNS extractor with its simple implementation consists of two-

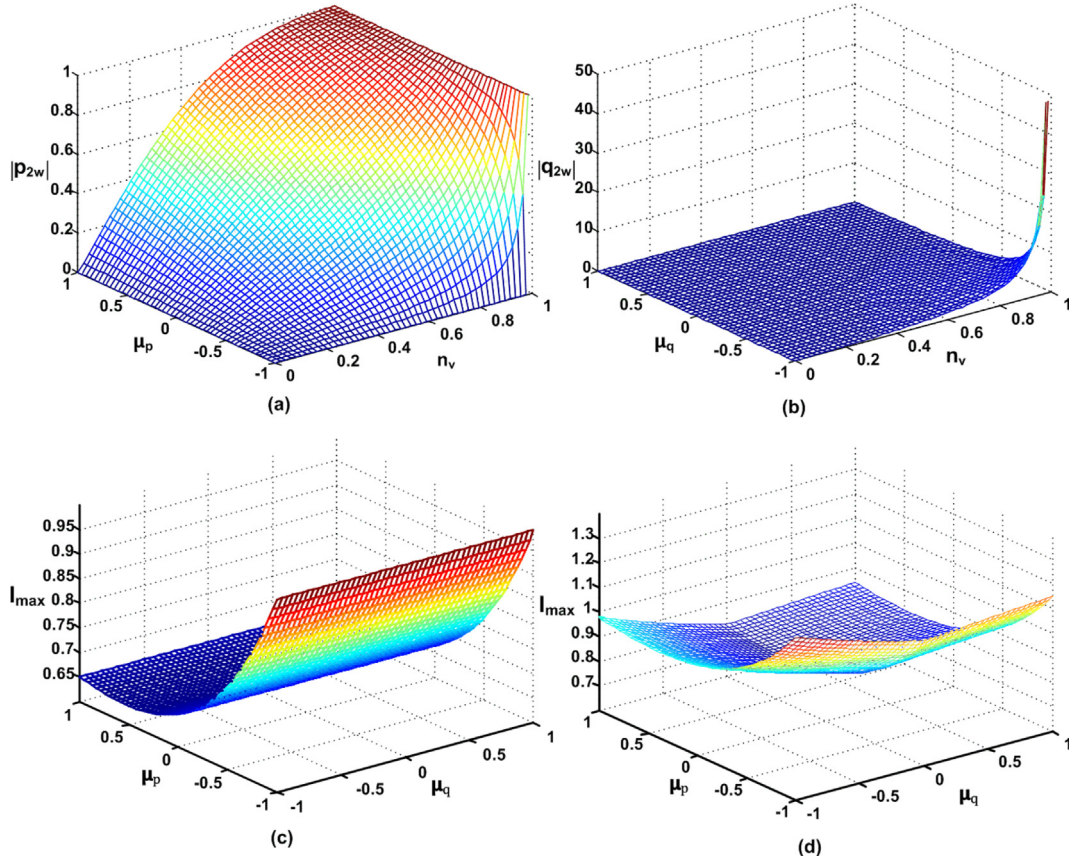


Fig. 1. Controllable parameters for: $|p_{2w}|$ (a) as function of μ_p and n_v , (b) $|q_{2w}|$ as function of μ_q and n_v , (c) maximum injected current as function of μ_p and μ_q with $I_q^* = 0$ and (d) maximum injected current with $I_q^* > 0$.

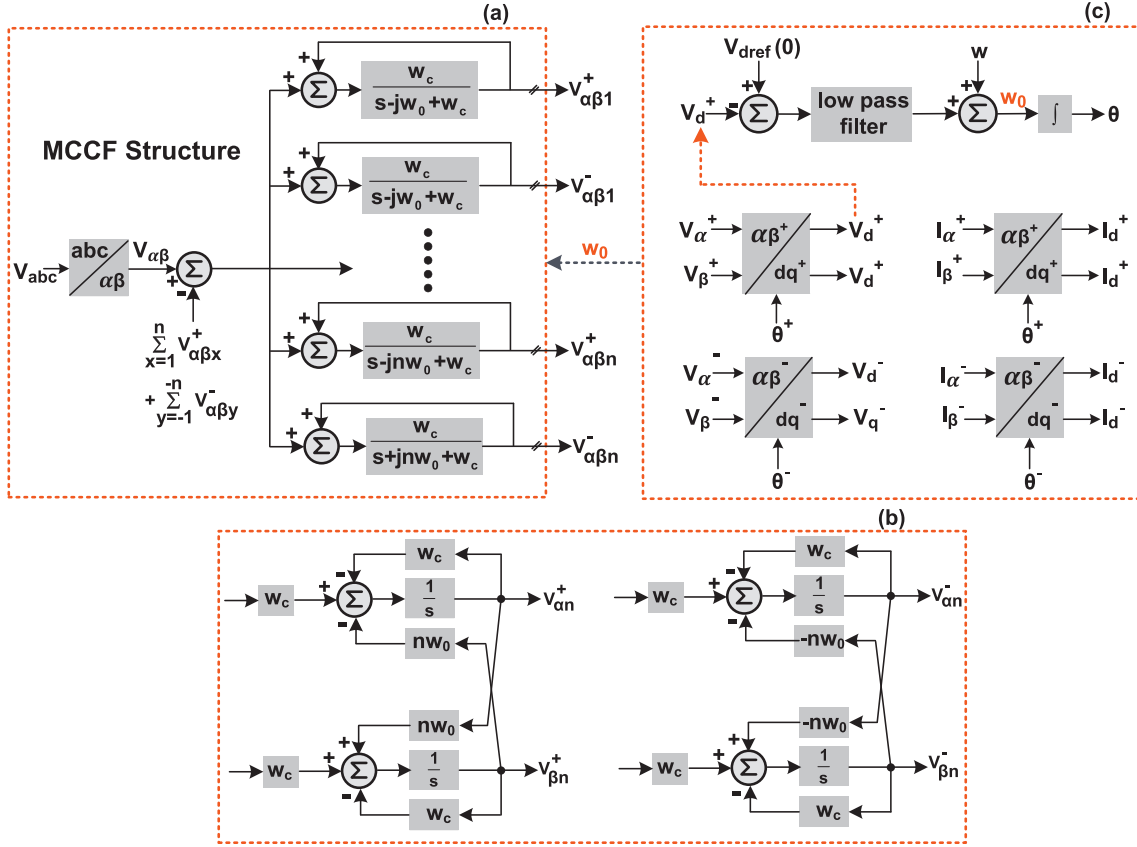


Fig. 2. The MCCF-PNS extractor; (a) MCCF structure; (b) sub-module of MCCF and (c) estimation phase angle and separation of PNS voltage-current components.

Table 1
Controllable of active-reactive oscillations based on μ_p parameter.

μ_p	$ p_{2\omega} $	$ q_{2\omega} $	Control target
1	$\frac{2P^* \ v^+\ \ v^-\ }{\ v^+\ ^2 + \mu_p \ v^-\ ^2}$	0	Q remains constant
0	$\frac{P^* \ v^+\ \ v^-\ }{\ v^+\ ^2 + \mu_p \ v^-\ ^2}$	$\frac{P^* \ v^+\ \ v^-\ }{\ v^+\ ^2 + \mu_p \ v^-\ ^2}$	balanced
-1	0	$\frac{2P^* \ v^+\ \ v^-\ }{\ v^+\ ^2 + \mu_p \ v^-\ ^2}$	P remains constant

average filter to minimize harmonic components instead of using multiple sub-modules in MCCF-PLL.

4.1. The MCCF based PNS extractor

The general structure of the multiple complex-coefficients filter-based (MCCF-PLL) consists of several complex-coefficient filters (CCFs) which work collaboratively [26,31]. The MCCF-PLL separate fundamental PNS and harmonic components and also provide fast dynamic response without using several Park transformations. Although it ensures some advantages than many advanced PNS extractor in literature, computational burden of MCCF-PLL still seems big problem and it is relatively affected unbalanced condition caused by voltage harmonics and grid faults. It is reported in [26] that the oscillations on PNS components are not completely solved. The MCCF structure is illustrated in Fig. 3. $V_{\alpha\beta 1}^+, V_{\alpha\beta 1}^-, \dots, V_{\alpha\beta n}^+, V_{\alpha\beta n}^-$ are represented the PNS and harmonic components. As sub module of MCCF, the transfer functions of CCF are given as follows;

$$CCF_{+n}(s) = \frac{w_c}{s - jw_0 + w_c}$$

$$CCF_{-n}(s) = \frac{w_c}{s + jw_0 + w_c} \tag{41}$$

where w_c is cut off frequency and w_0 is fundamental frequency that feedback to the MCCF. The MCCF model is developed by its mathematical model in PSCAD/EMTDC software. It can be seen that MCCF separate PNS voltage components with Eq. (42).

$$V_{\alpha 1}^+ = \frac{w_c}{s - jw_0 + w_c} \left[V_{\alpha} + V_{\alpha 1}^+ - \sum_{x=1}^n V_{\alpha x}^+ - \sum_{y=-1}^{-n} V_{\alpha y}^- \right]$$

$$V_{\beta 1}^+ = \frac{w_c}{s - jw_0 + w_c} \left[V_{\beta} + V_{\beta 1}^+ - \sum_{x=1}^n V_{\beta x}^+ - \sum_{y=-1}^{-n} V_{\beta y}^- \right]$$

$$V_{\alpha 1}^- = \frac{w_c}{s - jw_0 + w_c} \left[V_{\alpha} + V_{\alpha 1}^- - \sum_{x=1}^n V_{\alpha x}^- - \sum_{y=-1}^{-n} V_{\alpha y}^- \right]$$

$$V_{\beta 1}^- = \frac{w_c}{s - jw_0 + w_c} \left[V_{\beta} + V_{\beta 1}^- - \sum_{x=1}^n V_{\beta x}^- - \sum_{y=-1}^{-n} V_{\beta y}^- \right]$$

...

...

$$V_{\alpha n}^+ = \frac{w_c}{s - jw_0 + w_c} \left[V_{\alpha} + V_{\alpha n}^+ - \sum_{x=1}^n V_{\alpha x}^+ - \sum_{y=-1}^{-n} V_{\alpha y}^- \right]$$

$$V_{\beta n}^+ = \frac{w_c}{s - jw_0 + w_c} \left[V_{\beta} + V_{\beta n}^+ - \sum_{x=1}^n V_{\beta x}^+ - \sum_{y=-1}^{-n} V_{\beta y}^- \right]$$

$$V_{\alpha n}^- = \frac{w_c}{s - jw_0 + w_c} \left[V_{\alpha} + V_{\alpha n}^- - \sum_{x=1}^n V_{\alpha x}^- - \sum_{y=-1}^{-n} V_{\alpha y}^- \right]$$

$$V_{\beta n}^- = \frac{w_c}{s - jw_0 + w_c} \left[V_{\beta} + V_{\beta n}^- - \sum_{x=1}^n V_{\beta x}^- - \sum_{y=-1}^{-n} V_{\beta y}^- \right]$$

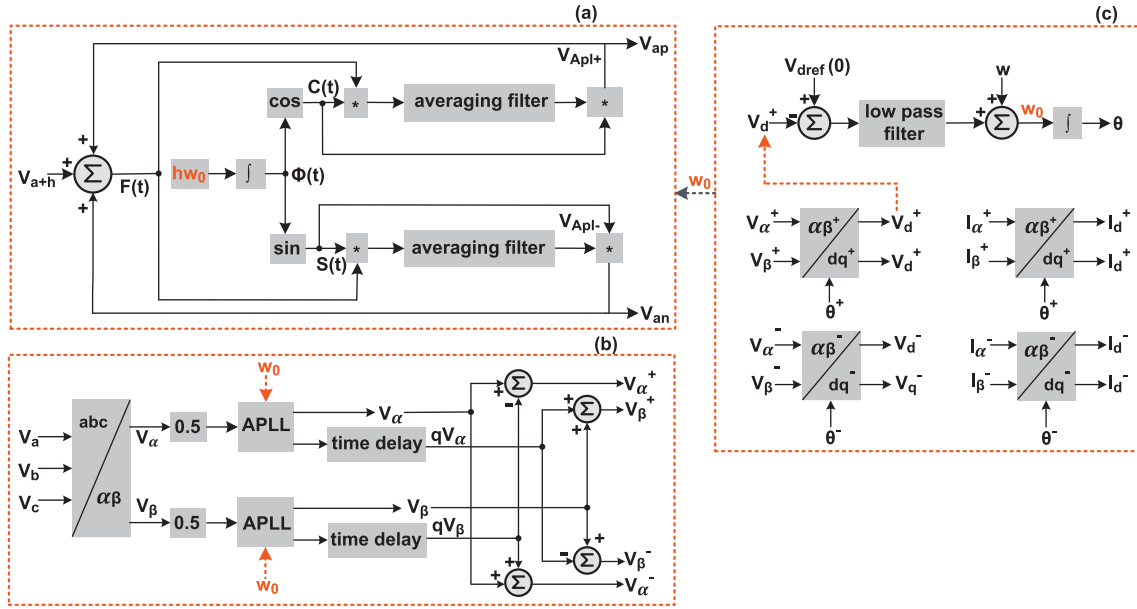


Fig. 3. The proposed PNS extractor; (a) single phase APLL, (b) improved DAPLL for PNS components and (c) estimation phase angle and separation of PNS voltage-current components.

4.2. The proposed PNS extractor

The Average filter based PLL (APLL) comprises of two average filters which are integrated into the simple structure of adaptive notch filter algorithm in [32]. Average Filter based PLL takes samples from the input signal in each period and computes the average of every sampling time. The phoneme is that the averaging of a sinusoidal signal gives a zero value. After Average filter processing, the distorted part of input signal is eliminated while DC part of the input signal is easily extracted [33]. Hence, the most significant feature of APLL has shorter synchronisation time and is less affected by voltage harmonics compared with advanced PLL in literature. It precisely extracts the amplitude, phase and PNS components and high order harmonics. In this paper, dual APLL (DAPLL) is proposed to extract fast and robust PNS voltage and current components under grid faults and harmonic distortions. Hence, PNS components are required to generate reference current. The measured PNS components from proposed DAPLL is embedded in RCG control module to deal with overcurrent phenomenon, to provide maximum power delivery and to minimize active and reactive power oscillations in GCI interfaced DG system. The proposed DAPLL removes both a double 2ω frequency oscillations (ripples) (caused by grid faults) and harmonic distortions (frequency ripples 6ω which is caused by low and high order harmonics). In this study, it is the first time that using only two APLL is integrated into three phase systems to produce PNS components. As shown Fig. 3, proposed DAPLL is applicable to both single phase signals and three phase signals. $V_a(t)$ or $V_{ApI+h}(t)$ represent grid phase voltage and consist of fundamental $V_a(t)$ or $V_{ApI}(t)$, harmonic voltage $V_h(t)$ and phase of input signal \varnothing_h can be written as follows [32];

$$V_{a+h}(t) = V_a + V_h = V_a \sin(\omega t + \varnothing_m) + \sum_{n=2}^{\infty} V_h \sin(h\omega t + \varnothing_h) \quad (43)$$

where h represent harmonic order. The fundamental voltages $V_a(t)$ consist of positive sequences $V_{ap}(t)$ and negative sequences $V_{an}(t)$ of voltages. The relationship between PNS voltages and input signal are given as follows [32];

$$V_a(t) = V_{ap}(t) + V_{an}(t) \quad (44)$$

Its feed-back signal $F(t)$ is obtained from PNS of input signal.

$$F(t) = V_{a+h}(t) + V_{ap}(t) + V_{an}(t) \quad (45)$$

Amplitude of PNS voltages are calculated from APLL;

$$|V_{ApI+}| = \frac{1}{T} \int_0^T C(t) \cdot F(t) \cdot dt = \frac{1}{T} \int_0^T \cos(h \cdot \varnothing(t)) \cdot F(t) \cdot dt = V_h \sin(\varnothing_h) \quad (46)$$

$$|V_{ApI-}| = \frac{1}{T} \int_0^T S(t) \cdot F(t) \cdot dt = \frac{1}{T} \int_0^T \sin(h \cdot \varnothing(t)) \cdot F(t) \cdot dt = V_h \cos(\varnothing_h) \quad (47)$$

For each harmonic at same time with its input phase signal is \varnothing_m ;

$$\varnothing_m = \tan^{-1} \left(\frac{|V_{ApI+}|}{|V_{ApI-}|} \right) \quad (48)$$

The PNS voltages with its amplitudes are written as follows;

$$V_{ap}(t) = |V_{ApI+}| \cdot C(t) = |V_{ApI+}| \cdot \cos(\omega t) \cdot \sin(\varnothing_m) \quad (49)$$

$$V_{an}(t) = |V_{ApI-}| \cdot S(t) = |V_{ApI-}| \cdot \cos(\omega t + \varnothing_m) \quad (50)$$

4.3. Proposed control structure

To generate firing signals of the GCI, the reference voltage signals V_{aref} and $V_{\beta ref}$ are obtained by proposed reference current signals in Eqs. (38) and (39) by processed FOPI controller. The FOPI controller is applied in Eqs. (51) and (52). Compared with conventional PI and PR controllers, the FOPI controller is preferred that can achieve zero steady-state error in STRF and ensures faster processing time. The reference voltages for firing signals of three phase inverter in STRF are obtained by Eqs. (51) and (52). The proposed entire test system is illustrated in Fig. 4.

$$\begin{aligned} V_{aref} &= [I_{aref} - I_{\alpha}] \cdot [FOPI] = [I_{aref} - I_{\alpha}] \cdot \left[k_p + \frac{k_i}{s^{\lambda}} \right] \\ V_{\beta ref} &= [I_{\beta ref} - I_{\beta}] \cdot [FOPI] = [I_{\beta ref} - I_{\beta}] \cdot \left[k_p + \frac{k_i}{s^{\lambda}} \right] \end{aligned} \quad (51)$$

$$\begin{aligned} V_{aref} &= \left[\frac{I_{aref}}{I_{max}} - I_{\alpha} \right] \cdot [FOPI] = \left[\frac{I_{aref}}{I_{max}} - I_{\alpha} \right] \cdot \left[k_p + \frac{k_i}{s^{\lambda}} \right] \\ V_{\beta ref} &= \left[\frac{I_{\beta ref}}{I_{max}} - I_{\beta} \right] \cdot [FOPI] = \left[\frac{I_{\beta ref}}{I_{max}} - I_{\beta} \right] \cdot \left[k_p + \frac{k_i}{s^{\lambda}} \right] \end{aligned} \quad (52)$$

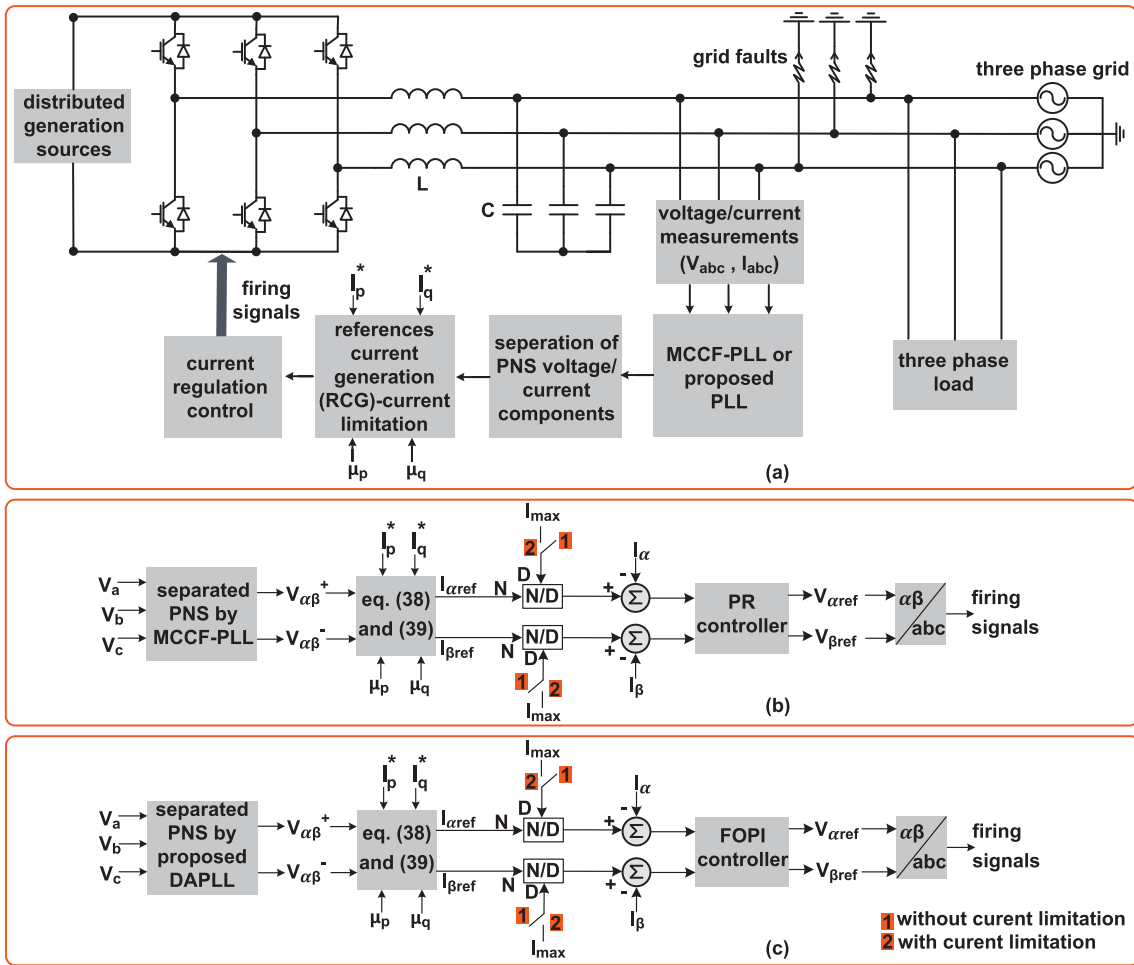


Fig. 4. Proposed entire system; (a) GCI interfaced DG system, (b) MCCF-PLL/PR based RCG controller and (c) proposed DAPLL/FOPI based controller.

where λ is positive real number for fractional order of integrator and k_p and k_i are proportional gain and integration gain, respectively. $I_{\alpha\beta\text{ref}}/I_{\text{max}}$ and $I_{\beta\text{ref}}/I_{\text{max}}$ represent current injection in stationary frame. While Eq. (51) does not deal with overcurrent, current limitation is surpassed by Eq. (52) in the proposed system.

5. Verification of proposed control structure

In this section, DG power system rated at 0.47 MW is built using PSCAD/EMTDC software. The DG energy sources are solar cell, wind turbine and fuel cell, which their rated powers are 0.117 MW, 0.11 MW and 0.29 MW, respectively. The performances comparison of proposed overcurrent limitation phenomenon is tested with MCCF-PLL based overcurrent limitation controller and previous similar studies. The main parameters for proposed test system are summarized in Table 2.

The proposed controller consists of four main parts:

- PNS extractor
- Current reference generator
- Current limitation control
- FOPI controller for AC current regulation

The 5th and 7th voltage harmonics and phase to phase grid fault are applied to the electric grid. At 0.3 s, phase B and C voltages are decreased at 65% of their nominal values. As depicted in Fig. 5, PNS voltage signals in stationary are extracted by proposed DAPLL and MCCF-PLL under heavily distorted grid conditions. It is clearly seen in Fig. 5 that proposed improved DAPLL minimized almost harmonic

Table 2
Parameters for proposed test system.

Parameters	Values	
Inverter input voltage	800 V	
Grid line-line voltage (rms)	380 V	
Grid frequency	50 Hz	
LC filter	L	0.5mH
	C	50uF
k_p	100	
k_i	10	
λ	0.5	
Switching frequency	2500 Hz	
Simulation parameters	Duration of run	1 s
	Solution time	0.025 ms
	Channel plot step	0.05 ms

contents on PNS voltage components in STRF at zero level by means of comparison of MCCF-PLL. While two filters are required for proposed DAPLL, multiple-modules are required for MCCF-PLL to deal with harmonic distortions.

The phase to phase fault conditions are applied to the three phase signals at 0.3 s during 0.2 s (ten cycles). The phase B and C voltages are decreased at 65% of their nominal values. The extracted PNS voltage components from MCCF-PLL and the proposed DAPLL are shown in Fig. 6. It is possible that although the MCCF-PLL achieves to extract fast PNS components in SRF, the amplitudes of PNS voltage signals have still oscillations. To highlight features of proposed PNS extractor, a cutaway-view is taken in Fig. 6. The proposed DAPLL with its simple

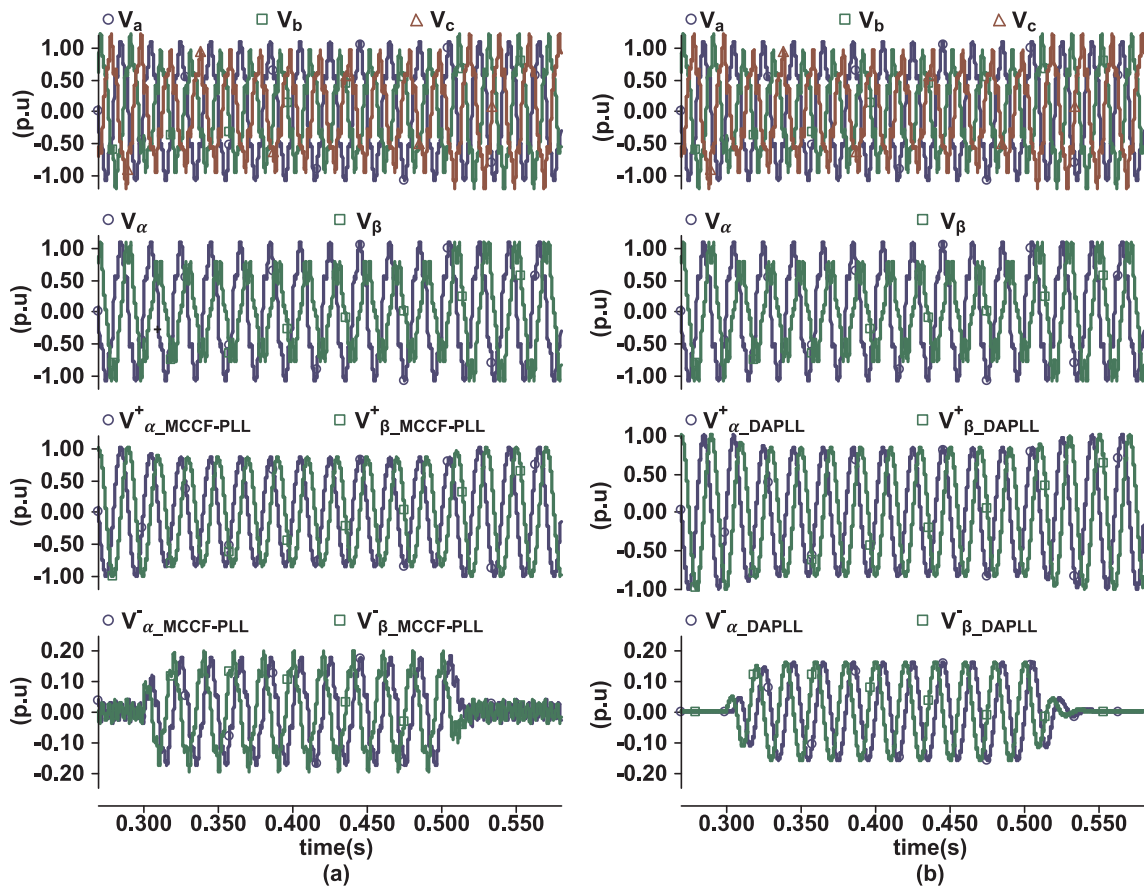


Fig. 5. MCCF-PLL and proposed DAPLL extract; (a) positive sequences and (b) negative sequences in STRF.

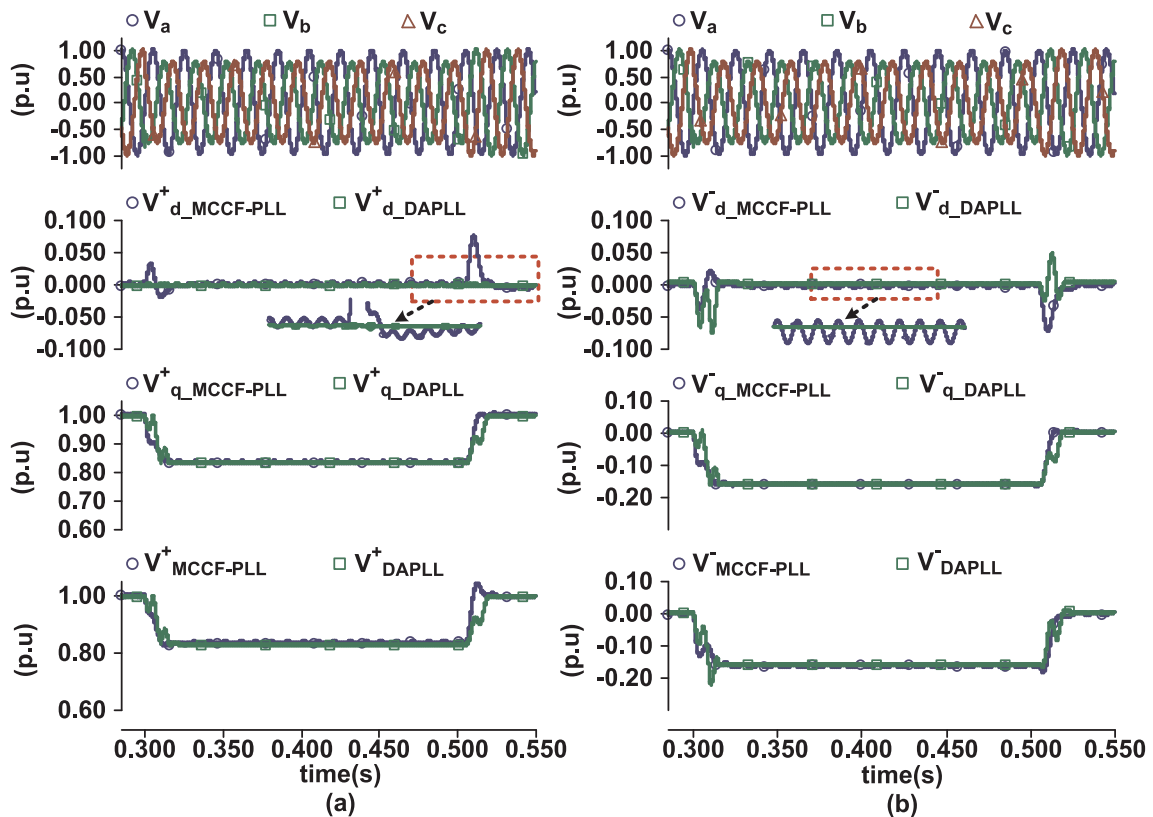


Fig. 6. MCCF-PLL and proposed DAPLL extract; (a) positive sequences and (b) negative sequences in SRF.

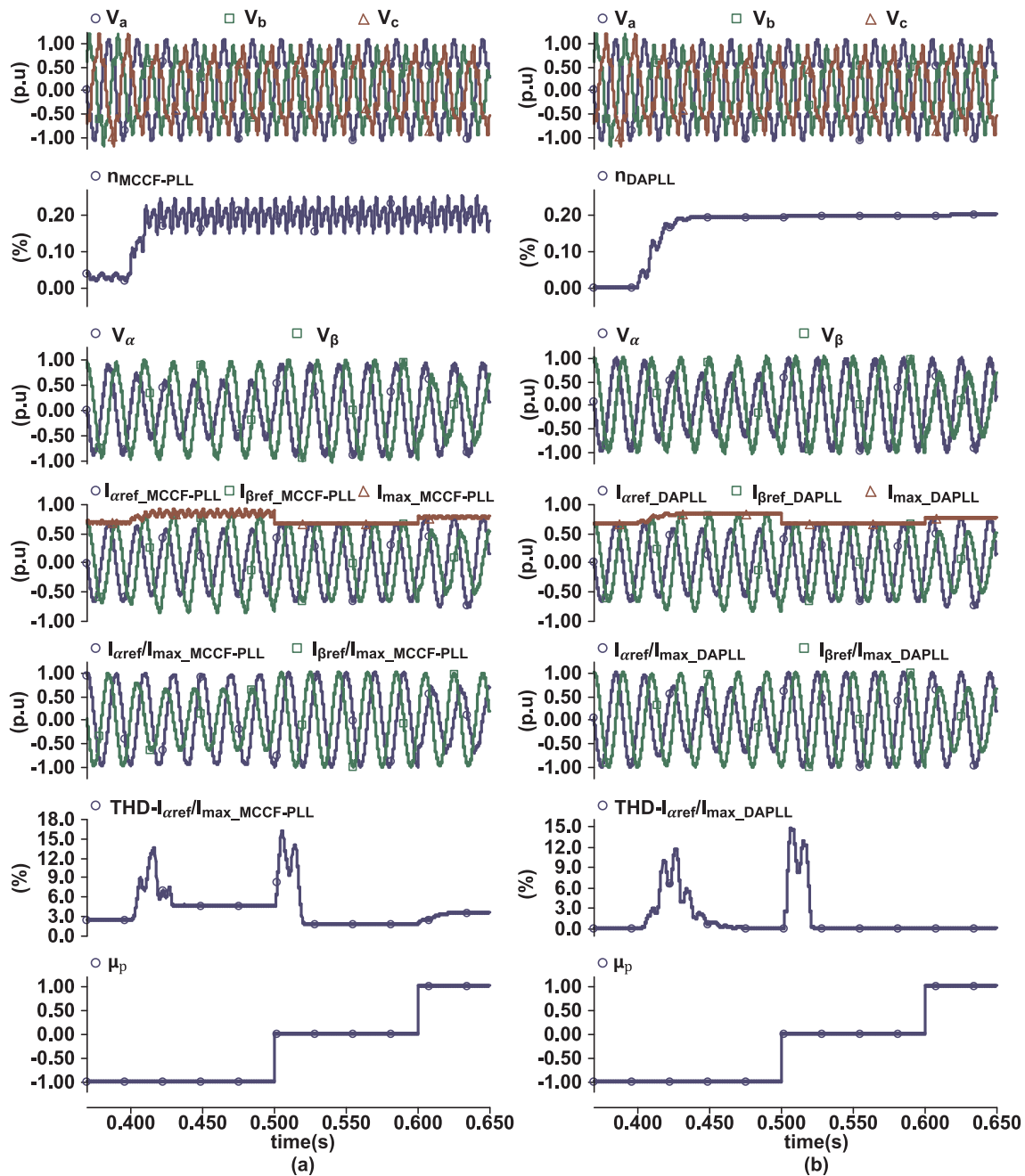


Fig. 7. The performances of RCG based on; (a) MCCF-PLL/PR controller and (b) proposed DAPLL/FOPI controller.

structure exhibits high performance and extracted fast and robust PNS components under distorted and unbalanced grid conditions. The dynamic response of proposed DAPLL is closer to the MCCF-PLL.

The PNS voltage and current components in STRF are separated by MCCF-PLL and improved DAPLL to generate reference current under grid faults and harmonic distortion in Fig. 7. After unbalanced and distorted grid voltages are occurred, the proposed DAPLL based current limitation controller provides less oscillations on voltage unbalanced factor n_v and maximum injected current I_{max} , injected current ($I_{\alpha ref}/I_{max}$ and $I_{\beta ref}/I_{max}$) in stationary frame than MCCF-PLL. It can be observed that the impact of voltage unbalance factor on MCCF-PLL include more oscillations on signals. The maximum injected current is tracking the reference current without any oscillations in middle of Fig. 7b. The injected current is in safety range for overcurrent prevention. The proposed controller achieves lower total harmonic distortion (THD), which is measured from injected current ($I_{\alpha ref}/I_{max}$ and $I_{\beta ref}/I_{max}$).

The phase to phase grid fault and 5th and 7th voltage harmonics are applied to the three phase signals at 0.4 s in Fig. 8. The MCCF-PLL based controller is considerably influenced by the voltage unbalance factor n_v and voltage harmonics. The positive and negative active and reactive power components p^+ , p^- , q^+ , q^- and amplitudes of active and reactive power oscillations for MCCF-PLL and DAPLL based control strategies $|p_{2w_MCCF-PLL}|$, $|q_{2w_MCCF-PLL}|$, $|p_{2w_DAPLL}|$ and $|q_{2w_DAPLL}|$ are flexibly adjusted with control parameter, μ_p . As shown in Fig. 8a, the MCCF-PLL based RCG controller does not overcome the oscillations on signals. In particular, despite the use of multiple-modules for rejection of harmonic distortion, it cannot deal with harmonics. As depicted in Fig. 8b, the proposed PNS extractor (DAPLL) based RCG controller ensures better solution to eliminate oscillations.

The MCCF-PLL/PR and the proposed DAPLL/FOPI control strategies are examined for overcurrent prevention under grid faults and harmonic distortion. Impact of harmonic distortions on control signals

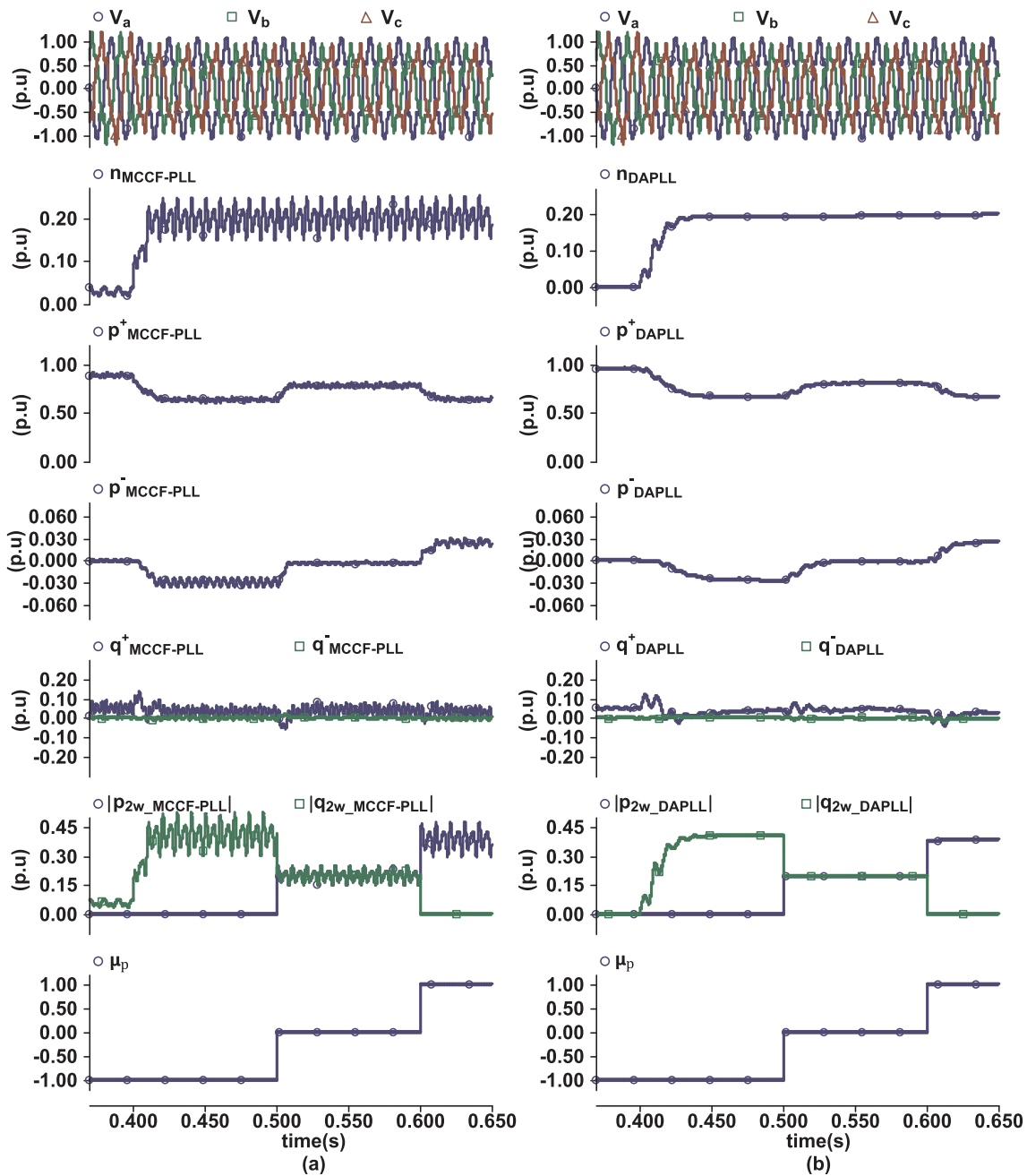


Fig. 8. The power oscillation analyses for RCG based on; (a) MCCF-PLL/PR controller and (b) proposed DAPLL/FOPI controller.

have not been taken into account in the previous similar control strategies. Many of them focus on grid faults. As shown Fig. 9, active and reactive powers are regulated with minimizing active and reactive power oscillations. Active power curtailment has been occurred to keep injected currents in safety limited range for both two controllers. However, the MCCF-PLL based RCG controller has high oscillations on signals and has high THD value for injected current. 5th and 7th harmonic orders for current phases A, B and C are plotted in Fig. 9a. The results clearly show that the proposed control strategy provides quite effective and robustness solution to minimize oscillations and low THD values for injected current. Fig. 9b depicts that current phases I_a , I_b and I_c have less than 0.5% THD values for the proposed control strategy. Harmonics of injected current I_a , I_b and I_c are extracted from 1st to 31st orders. As shown in Table 3, some numerical results are reported that proposed control strategy achieves lower THD values and individual harmonic contents compared with MCCF-PLL/PR controller.

At 0.4 s, single phase to ground fault is applied to three phase signals. The phase A to ground fault is occurred and its voltage is decreased at 50% of its nominal voltage. The performance of the RCG based on MCCF-PLL/PR and DAPLL/FOPI controller without current limitation are evaluated and plotted in Fig. 10a and 10b. The control parameter μ_p is changed from -1 to 1, linearly. The amplitudes of active and reactive power oscillations are flexibly adjusted with control parameters. When μ_p is -1, no active power oscillation, but reactive power oscillations are high. As μ_p is close to -1, active power oscillations increase and reactive power oscillations decrease and vice versa. Injected current is unbalanced with $\mu_p = \pm 1$. When μ_p is 0, oscillations occur on active and reactive powers and injected current is balanced. It can be observed from Fig. 10a and 10b that while injected currents for two controllers exceed the maximum constraint without current limitation ($I_{max} > I_{rated}$), the constant active power provides at inverter rated power. Hence, overcurrent phenomenon has been occurred. The

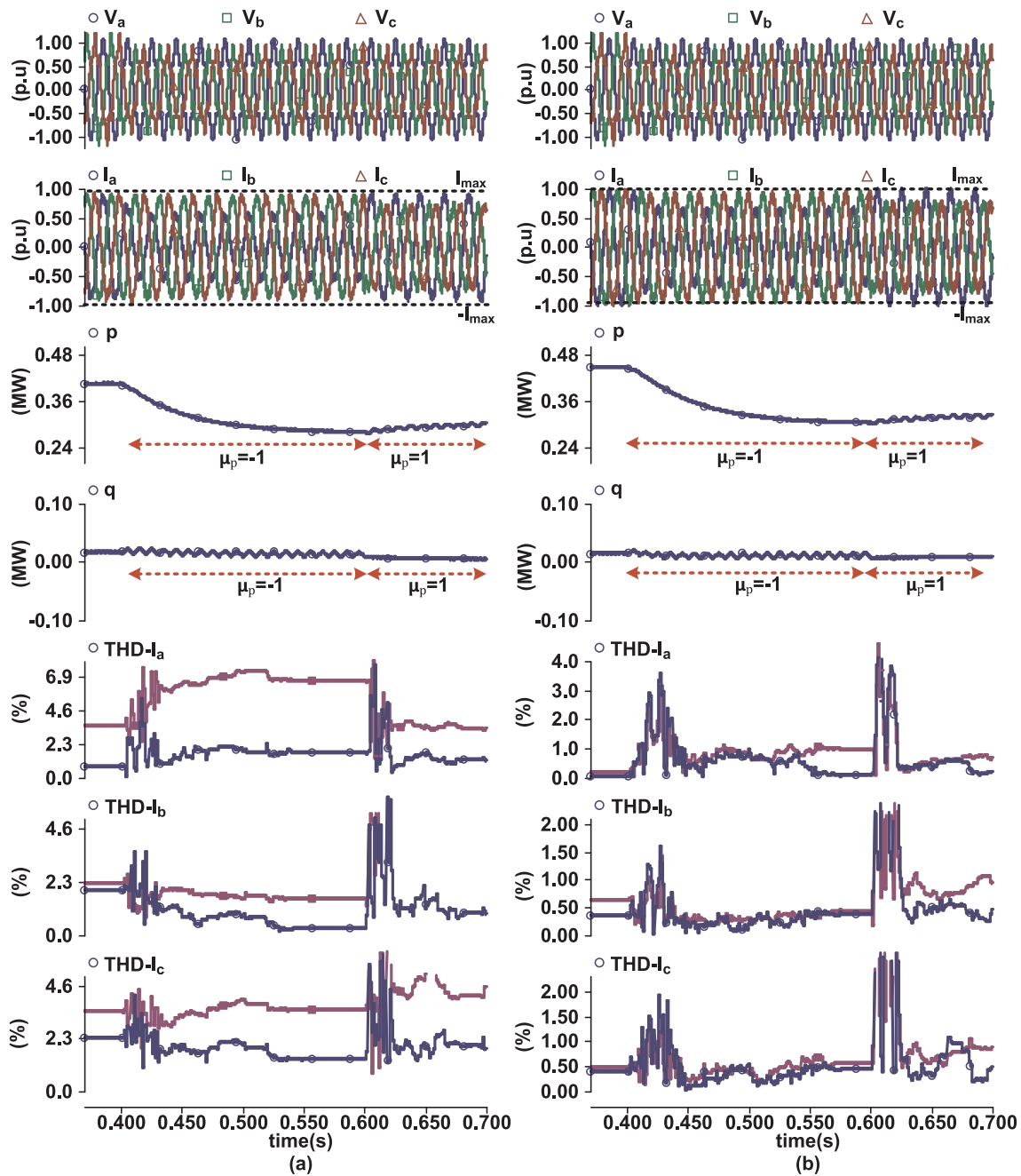


Fig. 9. The results for RCG based on; (a) MCCF-PLL/PR controller and (b) proposed DAPLL/FOPI controller.

Table 3
Performance comparison of control strategies under harmonic distortions.

Methods	phase A		phase B		phase C		THD (h = 31)		
	5th	7th	5th	7th	5th	7th	phase A	phase B	phase C
MCCF-PLL/PR controller	2.56%	1%	2.41%	1.86%	2.49%	2.33%	2.8%	3.1%	3.41%
Proposed control strategy	0.181%	0.101%	0.309%	0.109%	0.180%	0.066%	0.325%	0.35%	0.206%

results clearly prove that the rated active power can be maintained almost at its references. The DAPLL/FOPI controller ensures better solution to deal with oscillations by means of comparison of MCCF-PLL/PR controller. However, to avoid overcurrent phenomenon, active power curtailment must be occurred. As shown in Fig. 10c and d, it is clearly depicted that injected current is reduced in safety range limitation by RCG based MCCF-PLL/PR and proposed controllers. With the

proposed control strategy, it is observed that maximum injected current does not exceed the nominal current ($I_{max} < I_{rated}$) when compared to previous studies such as [27] and [34]. The proposed controller minimizes the oscillations on amplitudes of active-reactive power and orthogonal currents. The inverter rated power is smaller than its references during unbalanced grid faults.

As shown Fig. 11, proposed control strategy is capable of maximum

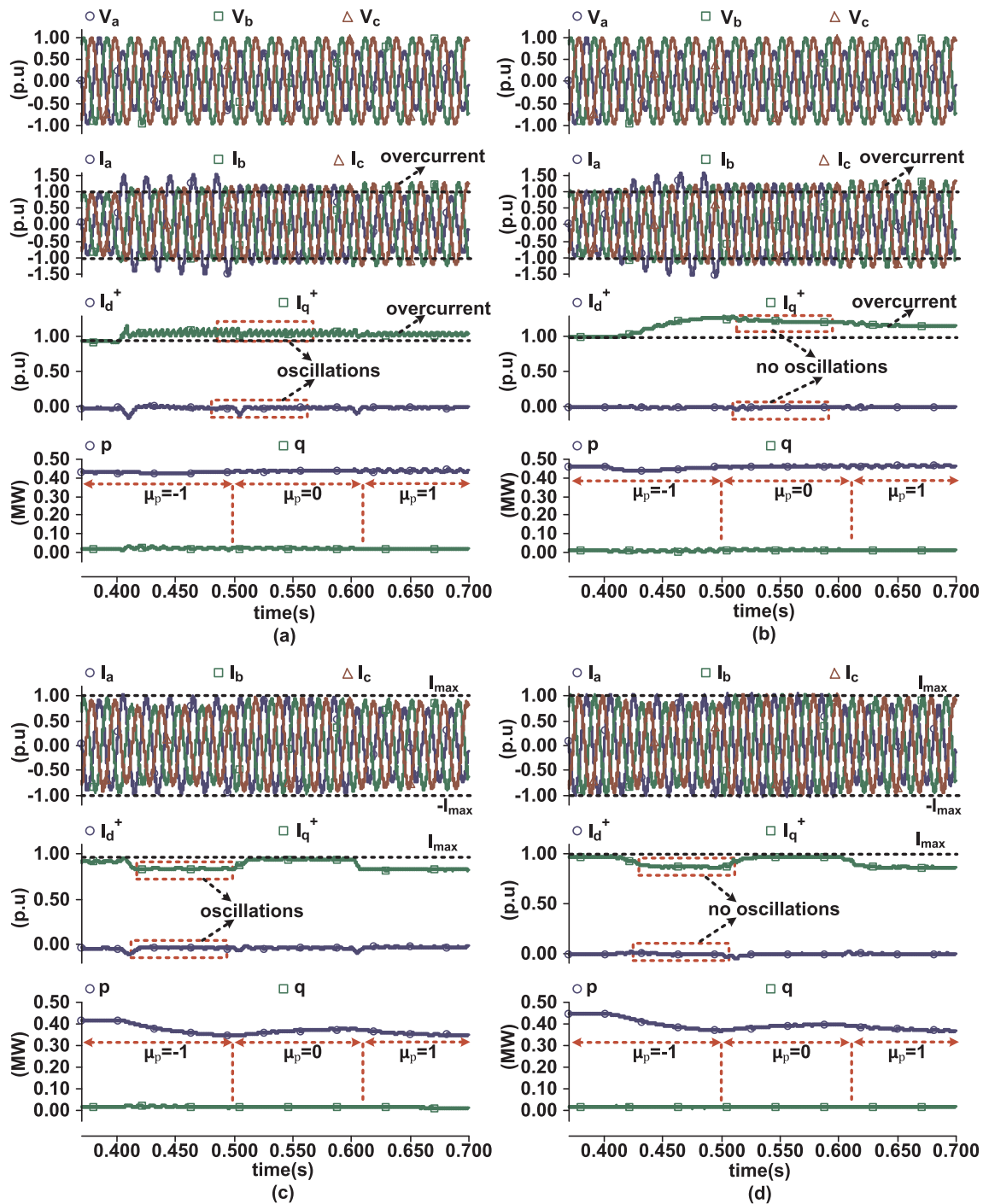


Fig. 10. The results for RCG based on; (a) MCCF-PLL/PR controller without current limitation, (b) proposed DAPLL/FOPi controller without current limitation, (c) MCCF-PLL/PR controller with current limitation and (d) proposed DAPLL/FOPi controller with current limitation.

limited current with various rated current (below 1 p.u) under grid faults. To observe the performances of proposed control strategy, various active power production scenarios are carried out. Firstly, Fig. 11a shows system considering high active power production $p = 0.47$ MW. During grid faults, maximum injected current does not exceed allowable phase currents $I_{max}(I_a, I_b, I_c) = I_{rated}$. Active power curtailment occurs from 0.47 MW to 0.232 MW. Secondly, medium active power production $p = 0.340$ MW is considered under same grid faults. As shown in Fig. 11b, $I_{max}(i^+) < I_{rated}$, $i^+ = 0.75$ p.u and active power curtailment occurs from 0.340 MW to 0.172 MW. Thirdly, low active power production $p = 0.22$ MW is considered in Fig. 11c. $I_{max}(i^+) < I_{rated}$, $i^+ = 0.5$ p.u and active power curtailment is performed

from 0.224 MW to 0.114 MW. Active power oscillations are eliminated as expected in three scenarios.

6. Discussion on performance comparison of proposed control strategy

To highlight the features of the proposed control strategy, several control strategies have been reported in the literature. Performance comparisons in terms of the regulation of active and reactive power, controllability of active and reactive power oscillations, current limitation phenomenon, AC current regulation control, number of control parameters and PNS extractors of control strategies are exhibited in

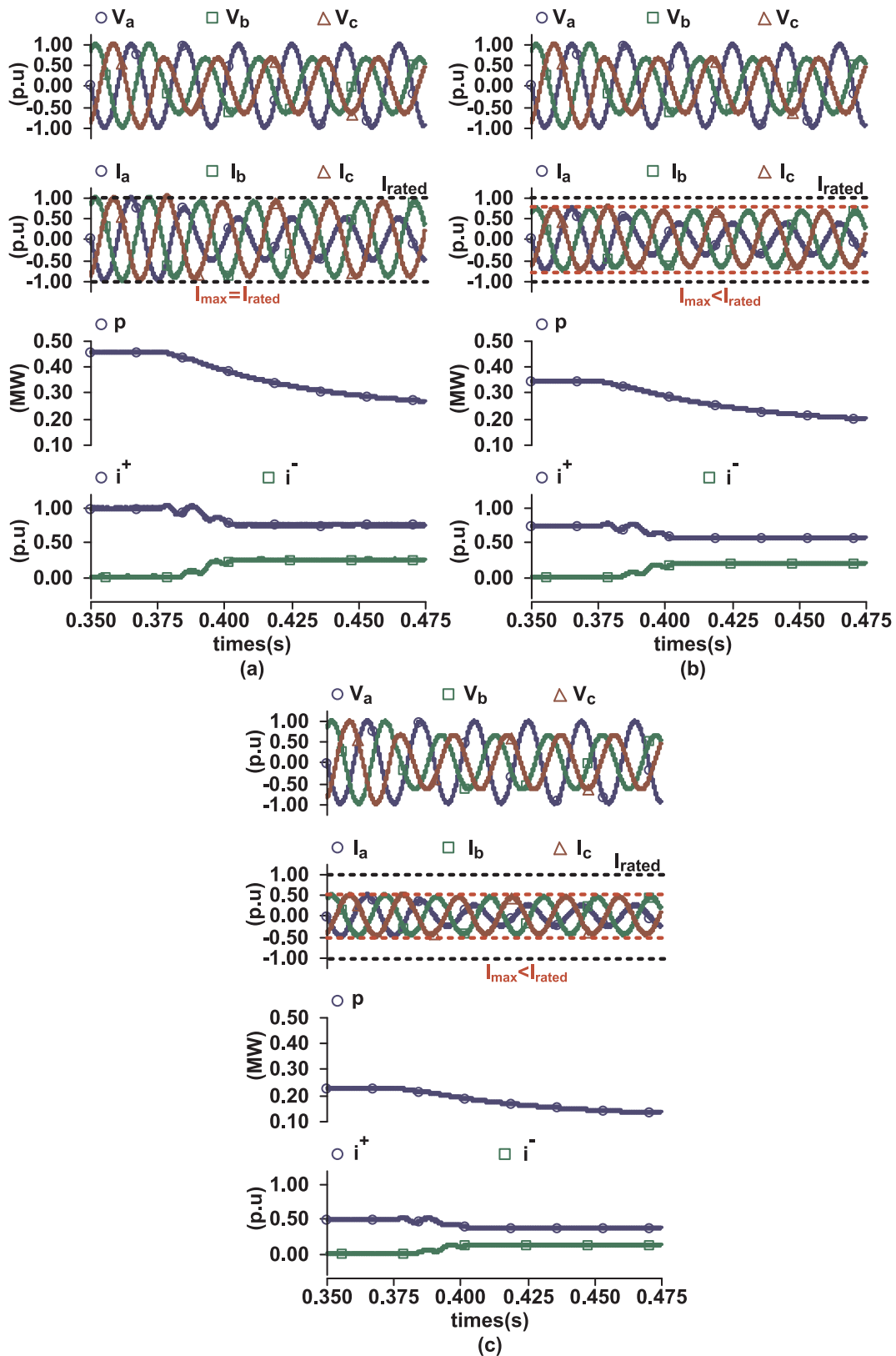


Fig. 11. The results for; (a) high injected current, (b) medium injected current, (c) low injected current.

Table 4. Some studies on regulation of active power P or reactive power Q , or both of P and Q , by generating the PNS current references have been reported in [5,6,9,14,20,27,34,35]. Active and reactive power are regulated, but control of active and reactive oscillations are not discussed in [5,20]. Another approach is mitigation of active-reactive

power oscillations. While some previous studies [5,20,23] have not dealt with both p_{2w} and q_{2w} oscillations, only active power oscillations are eliminated in [34,35]. Active and reactive power oscillations are discussed in [6,14], but current limitation control is not taken into considerations. The paper [27] and [35] examine current limitation

Table 4
Performance comparison of proposed control strategy.

Control strategy	Regulation of P, Q	Control of p_{2w} , q_{2w}	Current limitation	Current regulation	Number of FCP	PNS extractor
Ref. [5]	P	No	No	DB	No	DSOGI-PLL
Ref. [6]	P, Q	Yes	No	DSRF-PI	1	DSOGI-PLL
Ref. [9]	P, Q	Yes	Yes	PR	2	MCCF-PLL
Ref. [14]	P, Q	Yes	No	PR	1	MVF-PLL
Ref. [20]	P, Q	No	No	DSRF-PI	No	DSC-PLL
Ref. [23]	No	No	No	DDSRF-PI	No	DSRF-PLL
Ref. [27]	P, Q	Yes	Yes	PR	No	DSOGI-PLL
Ref. [34]	P, Q	only p_{2w}	No	PR	2	DSOGI-PLL
Ref. [35]	P, Q	only p_{2w}	Yes	PR	2	DSOGI-PLL
Proposed control strategy	P, Q	Yes	Yes	FOPI	1	DAPLL

phenomenon, but maximum methods. Because, a maximum injected current greater than rated current cause current magnitude control less restrictive. Moreover, the analytical expression of active and reactive power oscillations based on flexible control parameters are not examined as theoretically in [27]. To injected problem is the DSRF-PI [6,20] and DDSRF-PI [23] current regulators in synchronous are complex, consist of four PI controllers and need multiple reference frame transformations. To regulate PNS quantities, only two STRF based PR controllers are used in [9,14]. However, it is influenced by frequency variations and system parameters. While dead-beat (DB) controller [5] exhibits fast transient response, it is sensitive to model parameters. Other approach is number of flexible control parameters (FCP). Decreasing number of control parameters provide better controllability of oscillations. In these methods, impact of grid faults is only considered, performances of control strategy is not tested under harmonic distortions. As above mentioned in Introduction Section, PNS extractors are important part of control strategies. Proposed PNS extractor exhibits superior performance to previous methods.

As shown in Table 4, the main contributions of proposed control strategy comprises of: (1) active and reactive power regulation and minimizing active and reactive power oscillations with only one control parameters μ_p (it can be seen in Figs. 7–10), (2) maximum active power and minimum reactive power capability, (3) current limitation control for overcurrent protection, (4) compared with PI, PR, DB, DSRF-PI and DDSRF-PI current regulations, an advanced controller, FOPI is presented to regulate AC current, (5) compared with previous studies as above mentioned in Sections 1 and 4, fast and robust improved DAPLL based PNS extractor is presented.

7. Conclusion

A reference current generator (RCG) based proposed flexible power control strategy is presented to enable regulation of active and reactive power and minimizing active and reactive power oscillations under grid faults and harmonic distortions. The maximum current limitation control is inserted to the RCG to deal with overcurrent phenomenon. By introducing flexible RCG based the proposed controller enhances maximum active power and minimum reactive power transfer capability to electric grid and load without oscillations. With or without overcurrent limitation control, different injected current ratings have been also performed according to the various active power production scenarios.

The RCG is obtained from proposed DAPLL based PNS extractor which provides considerably fast dynamic response and is not almost influenced with voltage harmonics compared with previous similar studies. The performances of the proposed DAPLL based flexible control strategy are tested and compared with MCCF-PLL based control strategy. In particular, the proposed control strategy ensures lower THD value for injected current and better solution than MCCF-PLL based overcurrent limitation controller. Compared previous similar studies, impact of harmonic distortions on proposed control strategy is tested

and discussed. Instead of using PR in MCCF-PLL based controller, the FOPI controller achieves faster processing time, better and more accurate current regulation at steady state error in proposed solution. Theoretical analyses of active and reactive power oscillations are comprehensively deduced and discussed with flexible active-reactive power control and overcurrent limitation. Performance comparison of proposed control strategy are also comprehensively tested and over-viewed with previous studies. The effectiveness and robustness of the proposed solution has been verified by the simulation results and theoretical analysis.

References

- [1] Souza WF, De Lopes LAC. Power sharing control strategies for a three-phase microgrid in different operating condition with droop control and damping factor investigation. *IET Renew Power Gener* 2015;9(7):831–9.
- [2] Adefarati T, Bansal RC. Integration of renewable distributed generators into the distribution system: a review. *IET Renew Power Gener* 2016;10(7):873–84.
- [3] Gonçalves AFQ, Aguiar CR, Bastos RF, et al. Voltage and power control used to stabilise the distributed generation system for stand-alone or grid-connected operation. *IET Power Electron* 2016;9(3):491–501.
- [4] Darwish A, Massoud AM, Ahmed S. Single phase grid connected current source inverter: mitigation of oscillating power effect on the grid current. *Renewable Power Generation (RPG 2011)* 2011. p. 1–7.
- [5] Rodriguez P, Timbus AV, Teodorescu R, et al. Flexible active power control of distributed power generation systems during grid faults. *IEEE Trans Ind Electron* 2007;54(5):2583–92.
- [6] Kabiri R, Holmes DG, McGrath BP. Control of active and reactive power ripple to mitigate unbalanced grid voltages. *IEEE Trans Ind Appl* 2016;52(2):1660–8.
- [7] Heng T, Lajun CHEN, Yan GUO, et al. Flexible unbalanced control with peak current limitation for virtual synchronous generator under voltage sags. *J Mod Power Syst Clean Energy* 2018;6(1):61–72.
- [8] Jia J, Yang G, Nielsen AH. A Review on grid-connected converter control for short circuit power provision under grid unbalanced faults. *IEEE Trans Power Deliv* 2017;99:1–13.
- [9] Guo X, Liu W, Lu Z. Flexible power regulation and current-limited control of grid-connected inverter under unbalanced grid voltage faults. *IEEE Trans Ind Electron* 2017;64(9):7425–32.
- [10] Du X, Wu Y, Gu S, et al. Power oscillation analysis and control of three-phase grid-connected voltage source converters under unbalanced grid faults. *IET Power Electron* 2016;9(11):2162–73.
- [11] Camacho A, Castilla M, Miret J, et al. Active and reactive power strategies with peak current limitation for distributed generation inverters during unbalanced grid faults. *IEEE Trans Ind Electron* 2015;62(3):1515–25.
- [12] Nasiri M, Mohammadi R. Peak current limitation for grid side inverter by limited active power in PMSG-based wind turbines during different grid faults. *IEEE Trans Sustain Energy* 2017;8(1):3–12.
- [13] Montanari AA, Gole AM. Enhanced instantaneous power theory for control of grid connected voltage sourced converters under unbalanced conditions. *IEEE Trans Power Electron* 2017;32(8):6652–60.
- [14] Wang F, Duarte JL, Hendrix MAM. Design and analysis of active power control strategies for distributed generation inverters under unbalanced grid faults. *IET Gener Transm Distrib* 2010;4(8):905–16.
- [15] Sun LX, Chen Y, Wang Z, Ju P, et al. Optimal control strategy of voltage source converter-based high-voltage direct current under unbalanced grid voltage conditions. *IET Gener Transm Distrib* 2016;10(2):444–51.
- [16] Nejabatkhah F, Li YW, Wu B. Control strategies of three-phase distributed generation inverters for grid unbalanced voltage compensation. *IEEE Trans Power Electron* 2016;31(7):5228–41.
- [17] Wang D, Liu C, Li G. An optimal integrated control scheme for permanent magnet synchronous generator-based wind turbines under asymmetrical grid fault conditions. *Energies* 2016;9(4):1–27.
- [18] Rezaei MM, Soltani J. A robust control strategy for a grid-connected multi-bus

- microgrid under unbalanced load conditions. *Int J Electr Power Energy Syst* 2015;71:68–76.
- [19] Zhang W, Rocabert J, Candela JI, et al. Synchronous power control of grid-connected power converters under asymmetrical grid fault. *Energies* 2017;10(7):1–21.
- [20] Jin P, Li Y, Li G, Chen Z, et al. Optimized hierarchical power oscillations control for distributed generation under unbalanced conditions. *Appl Energy* 2017;194:343–52.
- [21] Chilipi R, Al Sayari N, Al Hosani K, et al. Third order sinusoidal integrator (TOSSI)-based control algorithm for shunt active power filter under distorted and unbalanced voltage conditions. *Int J Electr Power Energy Syst* 2018;96:152–62.
- [22] Ali Z, Christofides N, Hadjidemetriou L, et al. An advanced current controller with reduced complexity and improved performance under abnormal grid conditions. *PowerTech* 2017. p. 1–6.
- [23] Reyes M, Rodriguez P, Vazquez S, et al. Enhanced decoupled double synchronous reference frame current controller for unbalanced grid-voltage conditions. *IEEE Trans Power Electron* 2012;27(9):3934–43.
- [24] Tümay M, Meral ME, Bayindir KC. Sequence reference frame-based new sag/swell detection method for static transfer switches. *IET Power Electron* 2009;2(4):431–42.
- [25] Safa A, Berkouk EM, Messlem Y, Gouichiche A. A robust control algorithm for a multifunctional grid tied inverter to enhance the power quality of a microgrid under unbalanced conditions. *Int J Electr Power Energy Syst* 2018;100:253–64.
- [26] Guo X, Wu W, Chen Z. Multiple-complex coefficient-filter-based phase-locked loop and synchronization technique for three-phase grid-interfaced converters in distributed utility networks. *IEEE Trans Ind Electron* 2011;58(4):1194–204.
- [27] Todorović I, Grabić S, Ivanović Z. Grid-connected converter active and reactive power production maximization with respect to current limitations during grid faults. *Int J Electr Power Energy Syst* 2018;101:311–22.
- [28] Von Jouanne A, Banerjee B. Assessment of voltage unbalance. *IEEE Trans Power Deliv* 2001;16(4):782–90.
- [29] Taher SA, Karimi MH. Optimal reconfiguration and DG allocation in balanced and unbalanced distribution systems. *Ain Shams Eng J* 2014;5(3):735–49.
- [30] Castilla M, Miret J, Sosa JL, et al. Grid-fault control scheme for three-phase photovoltaic inverters with adjustable power quality characteristics. *IEEE Trans Power Electron* 2010;25(12):2930–40.
- [31] Li Y, Wang D, Han W, et al. Performance improvement of quasi-type-1 PLL by using a complex notch filter. *IEEE Access* 2016;4:6272–82.
- [32] Sarbulut L. A novel average filter based phase-locked loop for FACTS devices. *Electr Power Syst Res* 2016;136:289–97.
- [33] Meral ME, Çelik D. Benchmarking simulation and theory of various PLLs produce orthogonal signals under abnormal electric grid conditions. *Electr Eng* 2017;1–13.
- [34] Sosa JL, Castilla M, Miret J, et al. Control strategy to maximize the power capability of PV three-phase inverters during voltage sags. *IEEE Trans Power Electron* 2016;31:3314–23.
- [35] Lopez MAG, De Vicuna JLG, Miret J, et al. Control strategy for grid-connected three-phase inverters during voltage sags to meet grid codes and to maximize power delivery capability. *IEEE Trans Power Electron* 2018:1–15.